Electronic Supplementary Material (ESI) for Catalysis Science & Technology.
This journal is © The Royal Society of Chemistry 2017

**Electronic Supplementary Information (ESI)**

# Photocatalytic coupling of formaldehyde to ethylene glycol and glycoaldehyde over bismuth vanadate with controllable facets and cocatalysts

*Shunji Xie,[†] Zebin Shen,[†] Huamin Zhang, Jun Cheng, Qinghong Zhang,* and Ye Wang**

State Key Laboratory of Physical Chemistry of Solid Surfaces, Collaborative Innovation Center of Chemistry for Energy Materials, National Engineering Laboratory for Green Chemical Productions of Alcohols, Ethers and Esters, College of Chemistry and Chemical Engineering, Xiamen University, Xiamen 361005, China.

*CORRESPONDING AUTHOR: **E-mail:** wangye@xmu.edu.cn or zhangqh@xmu.edu.cn; **Phone:** +86-592-2186156; **Fax:** +86-592-2183047

[†]These authors contributed equally.

## Some Computational and Experimental Methods

**Computational Method.** All calculations were performed using DFT that was carried out with Dmol[3] Code. Exchange and correlation effects were described by the Perdew–Burke–Ernzerhof (PBE) within generalized gradient approximation (GGA).[1] The DFT semi-core pseudopotentials and DNP basis set were applied. In the structural optimizations all of the atoms were allowed to relax until the energy and forces are converged with tolerances of $2\times e^{-5}$ Ha and 0.004 Ha $Å^{-1}$ respectively. The mesh of k-points to sample the Brillouin zone was varied accordingly. In optimization of the unit cell of monoclinic scheelite $BiVO_4$ a k-point mesh of 6×6×3 was used. The lattice parameters after optimization for a conventional cell are a=5.2079Å, b=11.8785Å, c=5.1932Å and β=90°, which are close to the experimental data (standard card of PDF# 14-0688) and the lattice mismatch was less than 2%. A 2×2 supercell slab model was established for both $BiVO_4$ {010} and $BiVO_4$ {110} and a vacuum scale was set to 20 Å between repeated slabs. The lattice parameter of the optimized bulk was applied in the stoichiometric surface calculations. Monkhorst-Pack-type k-points samplings for $BiVO_4$ {010} and $BiVO_4$ {110} slabs were set 3×3×1. Considering the solvation effect, we adopt an implicit solvation model of the conductor-like screening model (COSMO).[2] With the adsorption of $Cl^-$ on $BiVO_4$ exposed facets under hydrothermal condition, $H^+$ was also adsorbed as counter ion to keep an electrically neutral system in our calculations. The adsorption of HCl was modelled on both sides of the slab for cancellation of surface dipoles and all the slab and adsorbate atoms were allowed to move during optimization. The surface energies ($\gamma$) of clean {010} and {110} surfaces and $Cl^-$-terminated {010} and {110} surfaces with different $Cl^-$ coverage were calculated by using the following equation:

$$\gamma = \frac{E^{slab} - nE^{bulk}_{BiVO_4} - n_H E_H - n_X E_X}{2A}$$

Where $E^{slab}$ refers to the total energy of the slab supercell, $n$ is the number of $BiVO_4$ units in the slab. $E^{bulk}_{BiVO_4}$ is the energy for bulk $BiVO_4$ per formula unit (f.u.), $E_H$ and $E_X$ refer the chemical potential of proton($H^+$) and halogen anion($X^-$), $n_H$ and $n_X$ are the number of adsorbed $H^+$ and $X^-$. A is the exposed area of the slab.

**Procedures for the synthesis of $BiVO_4$ using other Na-containing or Cl-containing salts instead of NaCl.** For other Cl-containing precursors, we used KCl, $CaCl_2$, $ZnCl_2$ or $AlCl_3$ to replace NaCl and kept the concentration of cationic ions identical to that of $Na^+$ ions. For other Na-containing precursors, we employed NaF, NaBr, NaI and $Na_2SO_4$ to replace NaCl and kept the concentration of anionic ions identical to that of $Cl^-$ ions. The other procedures were the same with those used for employing NaCl precursor.

**Procedures for the syntheses of $BiVO_4$-010 and $BiVO_4$-110.** For the synthesis of $BiVO_4$-010, $Bi(NO_3)_3 \cdot 5H_2O$ (5.0 mmol) was first dissolved into 10.0 mL aqueous solution of $HNO_3$ (4.0 mol $dm^{-3}$). $NH_4VO_3$ (5.0 mmol) was added into 10.0 mL aqueous solution of NaOH (2.0 mol $dm^{-3}$). Then, sodium

dodecyl benzene sulfonate (0.72 mmol) was added to the above solutions. After stirring for 0.5 h, the two solutions were mixed. The pH value of the mixed solution was adjusted to 7.0 with NaOH solution (2.0 mol $dm^{-3}$), and the mixture was stirred for 0.5 h. This mixture was transferred into a Teflon-lined stainless steel autoclave and was heated at 473 K for 1.5 h. The powdery sample was recovered by filtration, washing with deionized water and drying at 333 K in air overnight to obtain the $BiVO_4$-010 sample. The $BiVO_4$-110 sample was synthesized using a solid-liquid state reaction by mixing equal amount of $Bi_2O_3$ (2.5 mmol) and $V_2O_5$ (2.5 mmol) in 25 mL aqueous solution of $HNO_3$ (1.0 mol $dm^{-3}$). The mixture was stirred for 4 days at room temperature. The powdery sample was recovered by filtration, washing with deionized water and drying at 333 K in air overnight.

**Loading of Cocatalysts other than Pt, $MoO_x$ and $MnO_x$.** Metal oxide cocatalysts including $CrO_x$, $VO_x$, $WO_x$, $CuO_x$, and $FeO_x$ were loaded onto the 0.5 wt% Pt-$BiVO_4$-HT-50% by a photoreduction technique. In brief, $CrO_x$ species were deposited by photoreducing $K_2CrO_4$ in an aqueous solution containing methanol as a sacrificial agent under irradiation with a 300 W Xe lamp for 3 h. $Na_3VO_4$, $Na_2WO_4$, $Cu(NO_3)_2$ and $Fe(NO_3)_3$ were used as the precursors to replace $K_2CrO_4$ for the photodeposition of $VO_x$, $WO_x$, $CuO_x$ and $FeO_x$ onto Pt-$BiVO_4$, respectively.

Cocatalysts including $PbO_x$ and $CoO_x$ were loaded onto the $BiVO_4$-HT-50% by a photo-oxidation approach. For the loading of $PbO_x$, the $BiVO_4$-HT-50% was first dispersed in an aqueous solution of $Pb(NO_3)_2$ (0.10 M). After evacuation, the suspension was exposed to irradiation with a 300 W Xe lamp to deposit $PbO_x$ species. $NaIO_3$ with a concentration of 0.05 M was added into the suspension as an electron acceptor. After 3 h of photodeposition, the obtained sample was washed thoroughly with deionized water and dried overnight in vacuum. For the deposition of $CoO_x$ onto the $BiVO_4$-HT-50%, $Co(NO_3)_2$ was used as the precursor to replace $Pb(NO_3)_2$.

**Measurement of Apparent Quantum Yield.** We measured apparent quantum yields using UV light of 350 nm and visible light of 450 nm for the photocatalytic conversion of HCHO over the 3wt% $MnO_x$-3wt% $MoO_x$-0.5wt% Pt-$BiVO_4$-HT-50% catalyst. The apparent quantum yield ($\eta$) for the formation of a product was calculated using the following equation:

$$\eta = \frac{R(\text{electron}) \times N_A}{I(W/cm^2) \times S(cm^2) \times t(s) / E_\lambda(J)} \times 100\%$$

Where $N_A$, $I$, $S$, $t$ represent the Avogadro's constant, light intensity, irradiation area and reaction time, respectively. $E_\lambda$ can be calculated using $hc/\lambda$ ($\lambda$ = 350 or 450 nm). $R$(electron) represents the amount of electrons used in the formation of the products. $R_{EG}$(electron) and $R_{C2}$(electron) are the amounts of electrons used for the formations of EG and total $C_2$ compounds, respectively, and they can be calculated with the following equations: $R_{EG}(\text{electron}) = 2n(\text{EG})$ and $R_{C2}(\text{electron}) = 2n(\text{EG}) + 2n(CH_3CHO) +$

$n$(HOCH$_2$CHO), where $n$ is the amount of each product. The quantum yields for the formations of EG and total $C_2$ compounds can be calculated using $R_{EG}$(electron) and $R_{C2}$(electron), respectively.

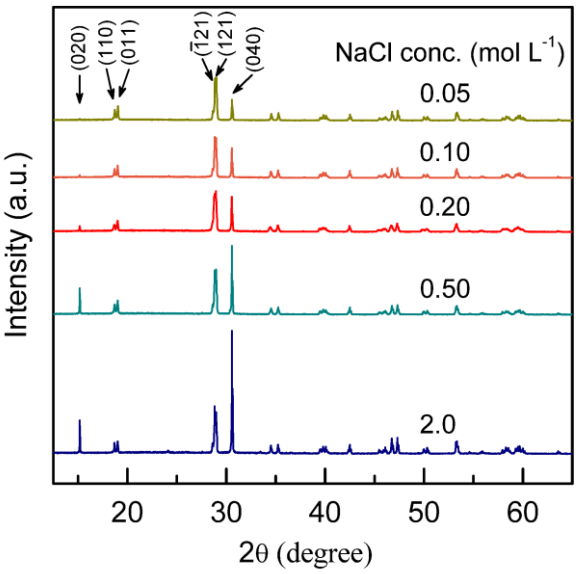


**Figure S1.** XRD patterns of $BiVO_4$ samples synthesized with different concentrations of NaCl.

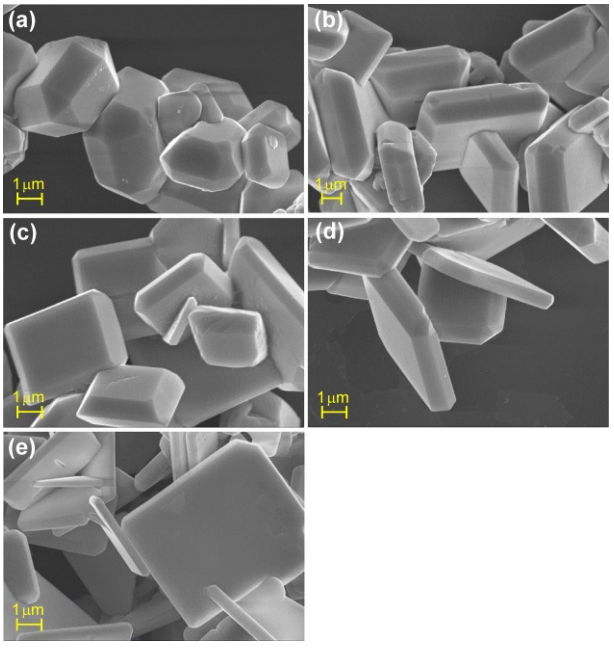


**Figure S2.** SEM micrographs of $BiVO_4$ samples synthesized with different concentrations of NaCl. NaCl concentration: (a) 0.050 M, (b) 0.10 M, (c) 0.20 M, (d) 0.50 M, (e) 2.0 M.

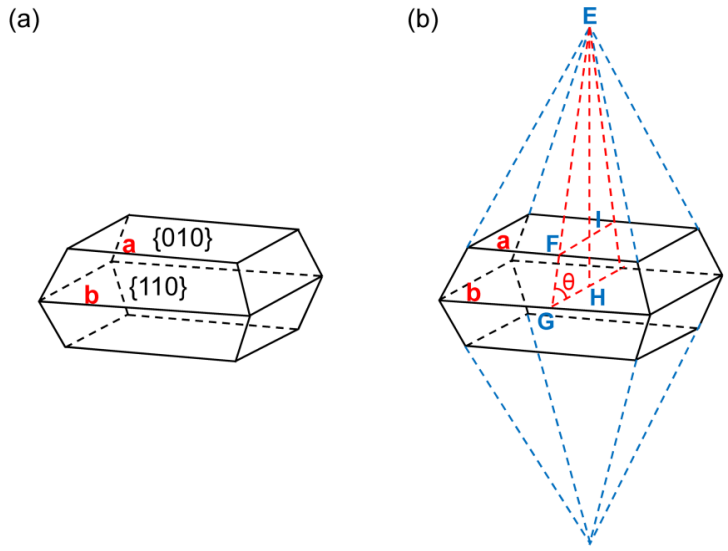


**Figure S3.** (a) Slab model of monoclinic $BiVO_4$ single crystal. (b) Equilibrium model of monoclinic $BiVO_4$ single crystal.

The percentages of {010} facets can be calculated as follows.[3,4]

$S_{010} = 2a^2$

$S_{110} = 8 \times 0.5 \times (a + b) \times FG$, $FG = EG - EF$, $EG = 0.5b / \cos\theta$, $EF = 0.5a / \cos\theta$

$S_{110} = 2 \times (b^2 - a^2) / \cos\theta$

$S_{010}\% = S_{010} / (S_{010} + S_{110}) = 2a^2 / [2a^2 + 2 \times (b^2 - a^2) / \cos\theta] = \cos\theta / (\cos\theta + b^2/a^2 - 1)$

Here θ is the theoretical value (66.07°) for the angle between the {010} and {110} facets of monoclinic $BiVO_4$. With the values of *b* and *a* measured from SEM, the percentages of {010} facets can be calculated from the above formula of $S_{010}\%$.

**Table S1.** Fraction of {010} facets of $BiVO_4$ single crystals synthesized with different concentrations of NaCl

| NaCl concentration (mol $L^{-1}$) | Mean size[c] (μm) | | {010}/{110} ratio | Fraction of {010} facets (%) |
|---|---|---|---|---|
| | *a* | *b* | | |
| 0.05 | 1.7 | 2.6 | 0.30 | 23 |
| 0.10 | 2.1 | 2.7 | 0.64 | 39 |
| 0.20 | 2.4 | 2.8 | 1.0 | 50 |
| 0.50 | 2.5 | 2.8 | 1.6 | 62 |
| 2.0 | 3.0 | 3.2 | 3.0 | 75 |

[c] The mean sizes of *a* and *b* were calculated from SEM micrographs by counting 100-200 particles.

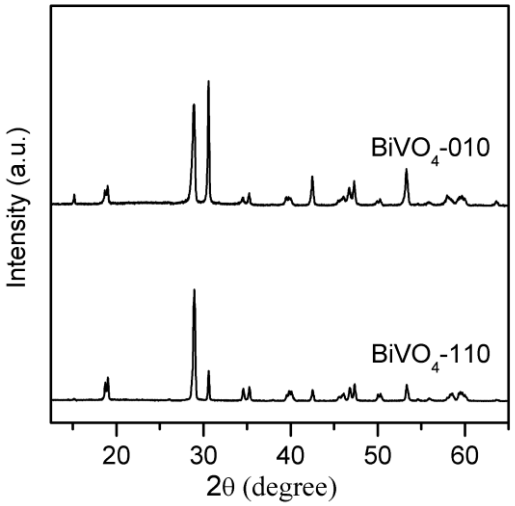


**Figure S4.** XRD patterns of $BiVO_4$-010 and $BiVO_4$-110.

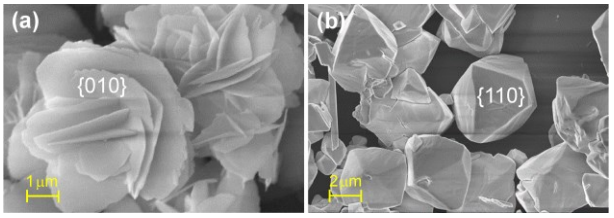


**Figure S5.** SEM micrographs of $BiVO_4$-010 and $BiVO_4$-110. (a) $BiVO_4$-010, (b) $BiVO_4$-110.

**Table S2.** Specific surface areas, mean sizes and bandgap energies of $BiVO_4$ single crystals with different fractions of exposed {010} facets

| Sample | Surface area ($m^2$ $g^{-1}$) | Mean size[a] (μm) | Bandgap energy[b] (eV) |
|---|---|---|---|
| $BiVO_4$-HT-23% | 2.6 | 2.6 | 2.3 |
| $BiVO_4$-HT-39% | 2.3 | 2.7 | 2.3 |
| $BiVO_4$-HT-50% | 2.1 | 2.8 | 2.3 |
| $BiVO_4$-HT-62% | 2.0 | 2.8 | 2.3 |
| $BiVO_4$-HT-75% | 1.9 | 3.2 | 2.3 |

[a] The mean size was calculated from SEM micrographs by counting 100-200 particles. [b] The bandgap energy was calculated from the diffuse-reflectance UV-vis spectra.

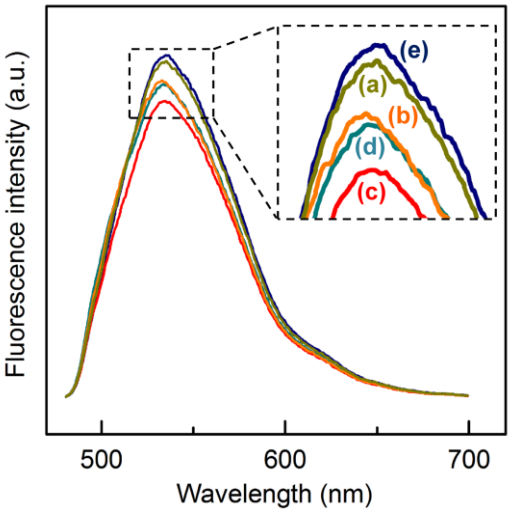


**Figure S6.** Photoluminescence spectra of $BiVO_4$ single crystals with different fractions of exposed {010} facets. (a) $BiVO_4$-HT-23%, (b) $BiVO_4$-HT-39%, (c) $BiVO_4$-HT-50%, (d) $BiVO_4$-HT-62%, (e) $BiVO_4$-HT-75%.

The intensity of the luminescence band at 535 nm, which was caused by the recombination of photogenerated electron-hole pairs, decreased in the order of $BiVO_4$-HT-75% > $BiVO_4$-HT-23% > $BiVO_4$-HT-39% > $BiVO_4$-HT-62% > $BiVO_4$-HT-50%. This suggests that the $BiVO_4$-HT-50% was the most efficient for the separation of photogenerated electron-hole pairs.

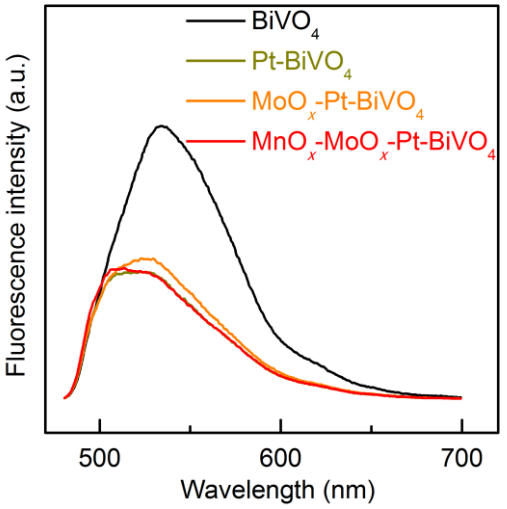


**Figure S7.** Photoluminescence spectra of $BiVO_4$-HT-50% with different co-catalysts.

The intensity of the luminescence band at 520-540 nm decreased significantly by deposition of Pt onto the $BiVO_4$-HT-50%, confirming the positive role of Pt in the separation of electron-hole pairs. The changes

of the luminescence intensity by loading $MoO_x$ and $MnO_x$ provided further evidence that $MnO_x$ had a positive effect, whereas $MoO_x$ was rather negative in the electron-hole separation.

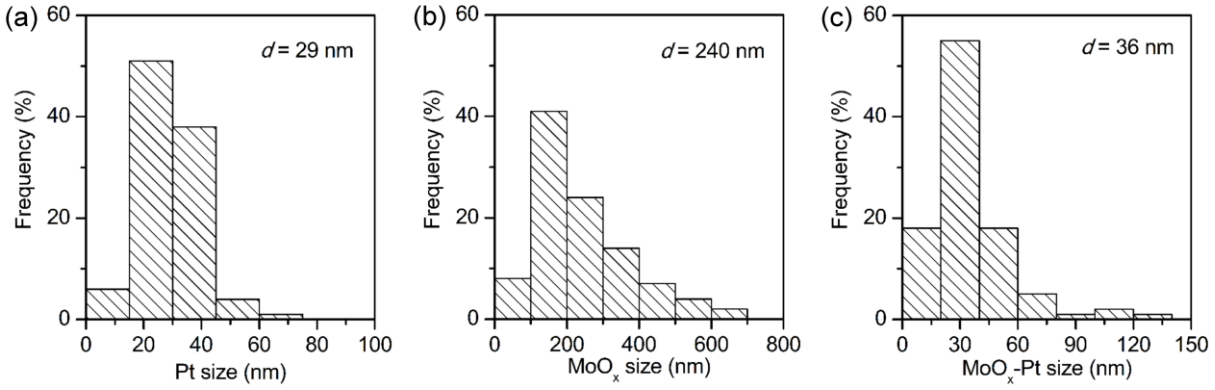


**Figure S8.** Distribution of sizes of particles photodeposited on {010} facets of $BiVO_4$ single crystals. (a) Pt particles on 0.5% Pt-$BiVO_4$-HT-50%, (b) $MoO_x$ particles on 3% $MoO_x$-$BiVO_4$-HT-50%, (c) $MoO_x$-Pt particles on 3% $MoO_x$-0.5% Pt-$BiVO_4$-HT-50%.

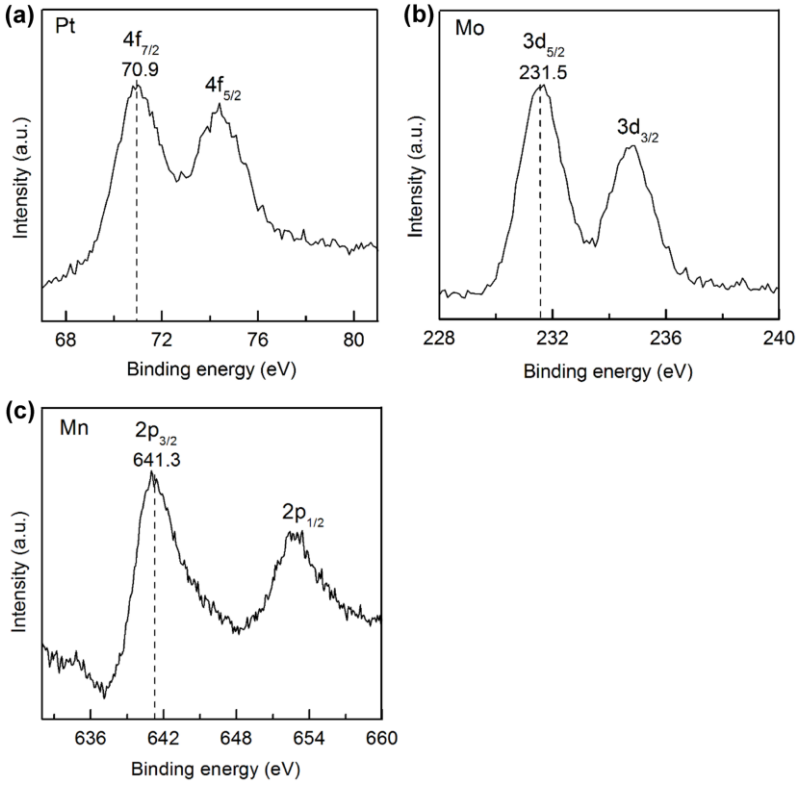


**Figure S9.** XPS spectra for 3% $MnO_x$-3% $MoO_x$-0.5% Pt-$BiVO_4$-HT-50% after light irradiation. (a) Pt 4f, (b) Mo 3d, (c) Mn 2p.

The catalyst after light irradiation was transferred into the detect chamber without exposure to air. The binding energy of Pt $4f_{7/2}$ was 70.9 eV, confirming that Pt was in metallic state in this sample.[5] The binding energy of Mo $3d_{5/2}$ for 3% $MnO_x$-3% $MoO_x$-0.5% Pt-$BiVO_4$-HT-50% was about 231.5 eV, which could be attributed to $Mo^V$.[6] The binding energy of Mn $2p_{3/2}$ (641.3 eV) suggested that Mn existed as $MnO_x$ ($1.5 < x < 2$) species on the surface of $BiVO_4$.[7]

## REFERENCES


1 J. P. Perdew, K. Burke and M. Ernzerhof, *Phys. Rev. Lett.*, 1996, **77**, 3865-3868.

2 B. Delley, *Mol. Simul.*, 2006, **32**, 117-123.

3 R. Li, F. Zhang, D. Wang, J. Yang, M. Li, J. Zhu, X. Zhou, H. Han and C. Li, *Nat. Commun.*, 2013, **4**, 1432.

4 J. Yu, J. Low, W. Xiao, P. Zhou and M. Jaroniec, *J. Am. Chem. Soc.*, 2014, **136**, 8839-8842.

5 L. Qiu, F. Liu, L. Zhao, W. Yang and J. Yao, *Langmuir*, 2006, **22**, 4480-4482.

6 K. Uchida and A. Ayame, *Surf. Sci.*, 1996, **357**, 170-175.

7 L. Ye, X. Liu, Q. Zhao, H. Xie and L. Zan, *J. Mater. Chem. A*, 2013, **1**, 8978-8983.